Supplementary Information for

"A percolation-based theoretical model reveals the structural origin of strain-stiffening in semiflexible fibrous networks"

Yi Zhou, Shuo Yang, Leitao Cao, Jing Ren, Runnan Bai, Yunhao Yang, Ruoxuan Peng, Jinrong Yao, Xin Chen, Zhengzhong Shao, and Shengjie Ling*

Supplementary Information contains:

Figure S1-S3

Note S1: Detailed derivation of the bending rigidity and persistence length

Note S2: The orientation-induced activation mapping and mode allocation

Note S3: Detailed derivation of the percolation threshold within the Erdős-Rényi model

Note S4: Apparent tangent-modulus and scaling analysis of the strain-stiffening

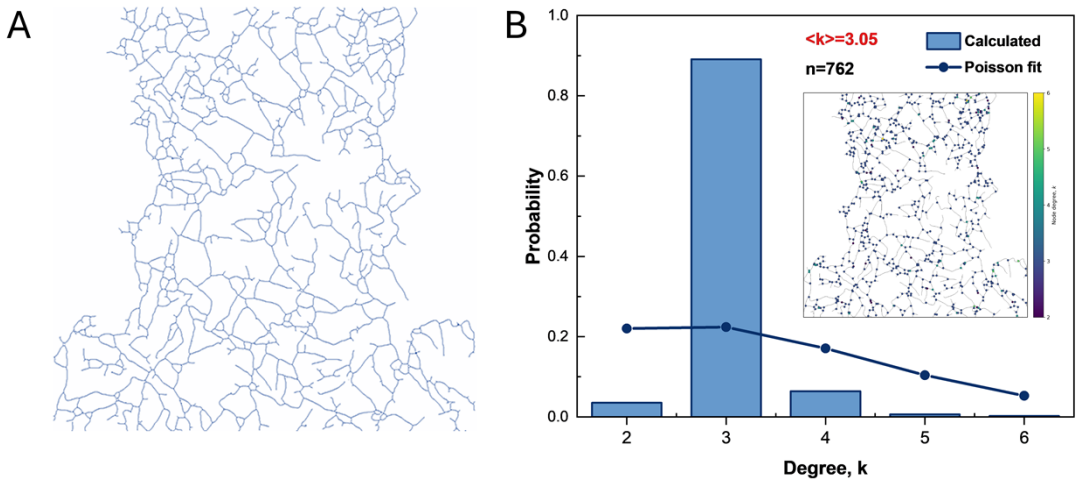

Fig.S1 The topology characteristics of silk nanofibril network extracted using the FN-DLS algorithm[1]. (A) skeletonized network (500 × 500-pixel image with one-pixel-wide skeleton lines) used for constructing the coarse-grained bead-spring model and (B) the corresponding node-degree distribution.

Note S1: Detailed derivation of the bending rigidity and persistence length

To estimate the effective stiffness of a semiflexible fiber in a bent state, based on classical beam elasticity theory, a fiber segment with a length of l_c and a bending stiffness of $k_b = EI$ can be approximated as a slender elastic Euler–Bernoulli beam. In the ideal case of a simply supported beam subjected to a transverse concentrated force F at its midpoint, the maximum midspan deflection is:

$$y_{L/2} = y_{\max} = \frac{Fl_c^3}{48EI}. \tag{S1}$$

The corresponding effective bending stiffness can be written as:

$$k_{eff} = \frac{F}{y_{L/2}} = \frac{48EI}{l_c^3}. \tag{S2}$$

It should be emphasized that this treatment is intended only to project the complex bent configuration of a fiber, in the small-deflection limit, onto its maximum fluctuation amplitude. It does not imply that fibers in the real network are subjected to a deterministic concentrated force at the midpoint, nor does it imply that the equivalent force arises solely from thermal fluctuations.

Within the two-dimensional framework, according to the equipartition theorem, the elastic potential energy in the harmonic approximation satisfies:

$$\langle E_{bend} \rangle = \frac{1}{2} k_{eff} \langle y_{L/2}^2 \rangle = \frac{1}{2} k_B T. \tag{S3}$$

Substituting eqn (S2) yields:

$$k_b = EI = \frac{l_c^3}{48} \cdot \frac{k_B T}{\langle y_{L/2}^2 \rangle}. \tag{S4}$$

However, k_b couples the fiber geometric parameter l_c with the constitutive parameter E. Its value therefore varies substantially with the sample-specific l_c, making it unsuitable for direct comparison among different fibers or across multiscale networks. To remove this geometric dependence and to map the mechanical-transition information encoded in fiber deformation back to an intrinsic material property, we further analyzed the relationship between the fiber persistence length l_p and Young's modulus E.

Following the theoretical framework proposed by Adamcik and Mezzenga for semiflexible protein nanofibrils[2,3], the persistence length l_p can be defined using the bond-correlation function as:

$$\langle t(s) \cdot t(0) \rangle = \exp\left(-\frac{s}{l_p}\right). \tag{S5}$$

Using small-angle approximation with $\kappa(s) = d\theta/ds$, we obtain the mean-square angular deviation:

$$\langle (\theta(s) - \theta(0))^2 \rangle = \frac{2\langle E_{\text{bend}} \rangle}{EI} \cdot s = \frac{k_B T}{EI} \cdot s, \tag{S6}$$

which leads to:

$$l_p = \frac{2EI}{k_B T}. \tag{S7}$$

Importantly, the prefactor reflects the intrinsic dependence of thermal energy distribution on spatial dimensionality. In 2D there is only one angular degree of freedom, giving:

$$\langle E_{\text{bend}}^{2D} \rangle = \frac{1}{2} k_B T, \tag{S8}$$

while in 3D there are two orthogonal bending degrees of freedom, giving:

$$\langle E_{\text{bend}}^{3D} \rangle = k_B T. \tag{S9}$$

Consequently,

$$k_b^{3D} = \frac{l_c^3}{24} \cdot \frac{k_B T}{\langle y_{L/2}^2 \rangle}, \tag{S10}$$

$$l_p^{3D} = \frac{EI}{k_B T}. \tag{S11}$$

It should be emphasized that the present theoretical framework is constructed from fiber contours and network skeletons extracted from AFM images. Accordingly, the relevant parameter definitions, model assumptions, and derivations are formulated within a two-dimensional framework.

Note S2: Orientation-induced activation mapping and mode allocation

Because the network's spatial arrangement combines orientational bias with segment discreteness, a macroscopic load generates highly non-uniform axial/bending responses at the single-fiber scale, placing different fibers into distinct mechanical states. Once the bending amplitude of sufficiently many fibers exceeds a threshold, the RPGC emerges and triggers a network-scale transition and structural evolution.

To relate fiber-level state transitions to network connectivity and to elucidate the mechanism of macroscopic stiffening, we first require an explicit $\tau(\varepsilon)$ that maps fiber-scale deformation statistics to network-scale measures.

Under the two-state framework derived from the single-bend hypothesis, we map uniaxial network deformation onto fiber-scale morphological and mechanical changes via an orientation-governed allocation scheme. This captures the nonlinear evolution from a compressive, bending-dominated regime to a tensile, load-bearing regime. At small strains, fiber deformation is dominated by bending: energy is stored primarily in flexure, and fibers furnish catenary-like geometric connections without transmitting axial stress. As strain increases, fibers gradually straighten and enter a tensile state that actively transmits load between nodes. Hence, the morphological change of the fiber is accompanied by the activation of its stress-transmission function. By converting macroscopic strain ε into the fraction of activated fibers, we map single-fiber morphological evolution to percolation-type connectivity statistics.

For consistency with the self-consistent network-scale equations used later, we express strains as engineering strains. Let the loading direction be the y-axis, the angle between a fiber and the y-axis be θ, and the lateral Poisson contraction be $-\nu\varepsilon$. The deformation gradient and right Cauchy–Green tensor are:

$$F = \begin{pmatrix} 1-\nu\varepsilon & 0 \\ 0 & 1+\varepsilon \end{pmatrix}, \tag{S12}$$

$$C = F^T F = \begin{pmatrix} (1-\nu\varepsilon)^2 & 0 \\ 0 & (1+\varepsilon)^2 \end{pmatrix}. \tag{S13}$$

For the determination of the Poisson's ratio ν, a reference value can be obtained by monitoring the transverse dimension of the central region of the fiber network during tensile simulation (Fig. S2A).

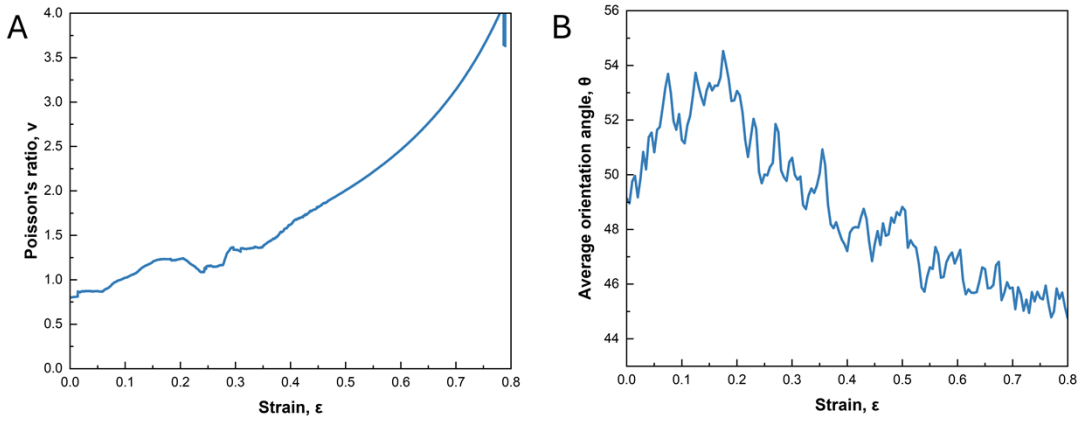

Fig. S2 The (A) apparent Poisson's ratio and (B) average orientation angle variation of the silk nanofibril network during uniaxial tensile simulation.

With the unit fiber direction $n(\theta) = (\sin\theta, \cos\theta)$, the principal stretch along the fiber is:

$$\lambda(\theta,\varepsilon) = \sqrt{n^T C\, n} = \sqrt{(1-\nu\varepsilon)^2 \sin^2\theta + (1+\varepsilon)^2 \cos^2\theta}. \tag{S14}$$

For analytical convenience, we further simplify the single-bend hypothesis as:

$$y(x) = A \cdot sin(kx), \quad A = y_{\frac{L}{2}}, \quad k = \frac{\pi}{\xi}, \quad x \in [0,\xi] \tag{S15}$$

.

In the small-slope limit,

$$l_c^{'} \approx \xi + \frac{1}{2}\int_0^{\xi} \left(\frac{dy}{dx}\right)^2 dx = \xi\left(1 + \frac{A^2k^2}{4}\right), \tag{S16}$$

$$\xi^{'} \approx \xi - \frac{1}{2}\int_0^{\xi} \left(\frac{dy}{dx}\right)^2 dx = \xi\left(1 - \frac{A^2k^2}{4}\right). \tag{S17}$$

Thus, in the compressive regime where $\lambda \in (0,1)$, the axial compression of a fiber becomes:

$$1 - \lambda = 1 - \frac{\xi^{'}}{\xi} = \frac{A^2k^2}{4} = \frac{\pi^2\delta^2}{4}, \quad \delta \equiv \frac{y_{L/2}}{\xi}, \tag{S18}$$

and the corresponding bending ratio is:

$$\tau^{'} = \frac{l_c^{'}}{\xi^{'}} = \frac{1+s}{1-s} = \frac{2-\lambda}{\lambda}, \quad s \equiv \frac{A^2k^2}{4} = 1 - \lambda \tag{S19}$$

.

Substituting the single-fiber activation criterion $\tau_{bend}^{*} \approx 1.1$ gives the corresponding principal-stretch threshold

$$\lambda^{*} = \frac{2}{1 + \tau_{bend}^{*}} \approx 0.95 \tag{S20}$$

.

As uniaxial stretching biases fiber orientations toward the loading axis, this criterion can be recast into a more intuitive cutoff-angle form:

$$\cos^2\theta_c^{*}(\varepsilon) = \frac{\lambda^{*\,2} - (1-\nu\varepsilon)^2}{(1+\varepsilon)^2 - (1-\nu\varepsilon)^2}, \quad 0 \le \theta_c^{*} \le \frac{\pi}{2}. \tag{S21}$$

Fibers with $\theta \leq \theta^*(\varepsilon)$ are mechanically activated and enter the tensile, load-transmission domain. It should be noted that τ_{bend}^* and θ_c^* are equivalent representations of the same criterion. Therefore, the criterion for determining $p(\varepsilon)$ is preferentially based on τ_{bend}^*, which is more readily monitored and statistically analyzed.

Considering the head–tail symmetry of fiber orientations with respect to the loading direction, we assume that the instantaneous fiber-orientation distribution follows a von Mises distribution:

$$\varphi(\theta \mid \kappa) = \frac{2e^{\kappa cos(2\theta)}}{\pi \cdot I_0(\kappa)}, \quad \theta \in \left[0, \frac{\pi}{2}\right], \tag{S22}$$

where I_0 is the modified Bessel function of the first kind (order zero), and κ measures orientational concentration. This distribution is used to approximate the gradual transition of fiber orientation from an isotropic state to an anisotropic state during tensile deformation. (The actual strain-dependent variation of the mean fiber-orientation angle is shown in Fig. S2B).

Since orientation evolves as an affine bias plus weak rotational diffusion at small strains, the order parameter $\langle \cos 2\theta \rangle$ grows approximately linearly with ε. We therefore adopt:

$$\kappa(\varepsilon) = \alpha\varepsilon, \tag{S23}$$

where α quantifies alignment sensitivity (set by material and network geometry). In addition, setting $\varepsilon = 0$ reveals the unconstrained initial state in which fiber orientations follow a uniform angular distribution with constant probability density $\frac{2}{\pi}$.

It should be emphasized that, in real networks, the orientations of individual fiber segments are constrained by nodal constraints, inter-fiber interactions, and other structural restrictions. Therefore, the introduction of the von Mises distribution serves only as an approximation for aiding physical interpretation and analytical formulation. When this theoretical framework is applied to predict the stress-strain response, $p(\varepsilon)$ should be obtained directly from the frame-by-frame MD statistics, based on the actual distribution of the fiber orientation angle θ or τ_{bend} relative to the prescribed threshold. Accordingly, the probability that a fiber remains compressive is:

$$f(\varepsilon) = \int_{\theta^*(\varepsilon)}^{\pi/2} \varphi(\theta \mid \kappa(\varepsilon)) d\theta, \tag{S24}$$

and the activation probability is:

$$p(\varepsilon) = 1 - f(\varepsilon) = \int_{0}^{\theta^*(\varepsilon)} \varphi(\theta \mid \kappa(\varepsilon)) d\theta. \tag{S25}$$

The cumulative compressive contribution to axial shortening from fibers that still store

bending energy at strain ε is:

$$C(\varepsilon) = \int_{\theta^*(\varepsilon)}^{\pi/2} [1 - \lambda(\theta,\varepsilon)]\varphi(\theta \mid \kappa(\varepsilon))\, d\theta \quad . \tag{S26}$$

Because $\kappa(\varepsilon)$ and $\theta^*_c(\varepsilon)$ are monotone, compressive fibers dominate at small strains. Hence, both $C(\varepsilon)$ and $\tau(\varepsilon)$ increase with ε until $\frac{dC}{d\varepsilon}|_{\varepsilon=\varepsilon_{c1}} = 0$. Beyond ε_{c1}, $f(\varepsilon)$ rapidly decreases (compressible fibers are depleted), and the network becomes predominantly tension-oriented and rigid. In this regime, with $f(\varepsilon_{c2}) = \eta \ll 1$, the response of $C(\varepsilon)$ vanishes while $\tau(\varepsilon)$ approaches a plateau τ_∞. At the network scale, ε_{c1} marks the percolation threshold and ε_{c2} shows the onset of steady constitutive behavior.

To obtain a more direct $\tau \sim \varepsilon$ relation, we define the mean axial compression among compressive fibers:

$$\bar{C}(\varepsilon) = \frac{C(\varepsilon)}{f(\varepsilon)} = \frac{\int_{\theta^*(\varepsilon)}^{\pi/2} [1 - \lambda(\theta,\varepsilon)]\varphi(\theta \mid \kappa(\varepsilon))\, d\theta}{\int_{\theta^*(\varepsilon)}^{\pi/2} \varphi(\theta \mid \kappa(\varepsilon)) d\theta} \quad . \tag{S27}$$

From eqn (S18), the statistically defined effective bending amplitude over the compressive domain is:

$$\delta_{\text{eff}}(\varepsilon) = \frac{2}{\pi}\sqrt{\bar{C}(\varepsilon)} = \frac{2}{\pi}\sqrt{\frac{C(\varepsilon)}{f(\varepsilon)}}\,, \tag{S28}$$

Substituting δ_{eff} into eqn (17) yields the τ-ε mapping:

$$\begin{aligned} \tau(\varepsilon) &= \tau_{\text{bend}}[\delta_{\text{eff}}(\varepsilon)] = \frac{2}{\pi}\sqrt{1+\pi^2\delta_{eff}^2}\, E\left(\frac{\pi^2\delta_{eff}^2}{1+\pi^2\delta_{eff}^2}\right) \\ &= \frac{2}{\pi}\sqrt{1+4\bar{C}(\varepsilon)}\, E\left[\frac{4\bar{C}(\varepsilon)}{1+4\bar{C}(\varepsilon)}\right]. \end{aligned} \tag{S29}$$

In the small-strain limit ($\bar{C} \ll 1$), a first-order expansion gives:

$$\tau(\varepsilon) \approx 1 + \bar{C}(\varepsilon) = 1 + \frac{C(\varepsilon)}{f(\varepsilon)}\,, \tag{S30}$$

which explains the synchronous increase of τ and C in the initial strain regime and fixes the proportionality.

Note S3: Detailed derivation of the percolation threshold within the Erdős-Rényi model

Within the framework in which the Erdős-Rényi (ER) model is adopted as a mean-field connectivity reference for the real fibrous network, the nodal degree k is approximated as following a Poisson distribution with mean degree z:

$$\langle k \rangle = z, \quad P(k) \approx \frac{z^k e^{-z}}{k!}. \tag{S31}$$

The corresponding probability-generating function (PGF) of the degree distribution is therefore given by:

$$G_0(x) = \sum_{k=0}^{\infty} P(k) x^k = e^{-z(1-x)}. \tag{S32}$$

When a node is reached by following a randomly selected original edge, the number of its remaining connections, excluding the incoming edge, follows the excess-degree distribution. The corresponding probability-generating function is:

$$G_1(x) = \frac{G_0'(x)}{G_0'(1)}. \tag{S33}$$

Based on this definition, let u denote the probability that, after following a randomly selected original edge, the path does not lead to the rigidity-percolation giant component (RPGC). This event can occur in two mutually exclusive ways. First, the connectivity of the selected edge is not activated, with probability $1-p$. Here, the activation probability p corresponds to the fraction of fibers that are identified, according to the τ_{bend}^{*} criterion in the main text, as being in a stretched and stress-transmitting state. Second, the selected edge is activated, with probability p, but the node reached through this edge cannot connect to the RPGC through any of its remaining edges. The probability of this latter event is given by $G_1(u)$. Therefore, the following self-consistent equation is obtained:

$$u = (1-p) + pG_1(u). \tag{S34}$$

For a Poisson degree distribution, substitution into the above expression gives $G_1'(1) = z$. Thus, its degree-generating function and the excess-degree-generating function take the same form:

$$G_1(x) = G_0(x) = e^{-z(1-x)}. \tag{S35}$$

And eqn (S34) can be simplified to the explicit form:

$$u = (1-p) + pe^{-z(1-u)}. \tag{S36}$$

For this equation, if the trivial solution $u = 1$ always exists, it indicates that a path starting from any branch cannot reach the RPGC and that the network therefore does not form a percolated structure. To determine whether a non-trivial solution with $u < 1$ emerges, we define the right side of eqn (S34) as:

$$f(u) = (1 - p) + pG_1(u). \tag{S37}$$

Linearizing $F(u)$ about the trivial fixed point $u = 1$ gives:

$$f'(1) = pG_1'(1) = pz, \tag{S38}$$

Thus, the percolation threshold corresponds to the point at which stability changes, namely when:

$$p_c = \frac{1}{z}. \tag{S39}$$

It should be emphasized that the above derivation is only a mean-field approximation based on the ER random-network model. It implicitly assumes a Poisson degree distribution and the absence of spatial correlations, and therefore should not be interpreted as a strict prediction of the percolation threshold of the real fibrous network. For the actual fibrous network reconstructed from AFM images, a more appropriate approach is to construct $G_0(x)$ and $G_1(x)$ directly from the experimentally measured nodal degree distribution $P(k)$.

Note S4: Apparent tangent-modulus and scaling analysis of the strain-stiffening

To further examine the strain-stiffening behavior, we calculated the apparent tangent modulus, $K = d\sigma/d\varepsilon$, from the simulated stress–strain curve and performed an apparent scaling analysis. As shown in Fig. S3A, K starts to increase noticeably at $\varepsilon \approx 0.22\sim0.25$. This strain range is consistent with the onset window of the rigidity percolation giant component (RPGC) identified in the main text, as well as the non-affine-to-affine transition region. It supports the interpretation that the stiffening onset is associated with the emergence of a percolated load-bearing backbone rather than a singular instability of individual fibers.

When $K$is plotted as a function of stress, a short crossover regime is observed near the stiffening onset, followed by a broad plateau-like region (Fig. S3B). A log–log representation of K versus σ gives an apparent scaling exponent of approximately $\alpha \approx 0.24$ over the stiffening window (Fig. S3C). However, because the stress range available for fitting is limited and the network is reconstructed from a finite AFM-derived structure, this value should not be regarded as a universal critical exponent. Moreover, the present simulations do not explicitly include soft-mode fluctuation contributions[4]. Therefore, the observed strain-stiffening behavior should not be interpreted as a fully established finite-temperature critical phenomenon[5,6]. Instead, this theoretical model can be used as diagnostic evidence for a material-specific, percolation-like stiffening onset associated with the formation of an RPGC-dominated load-bearing backbone.

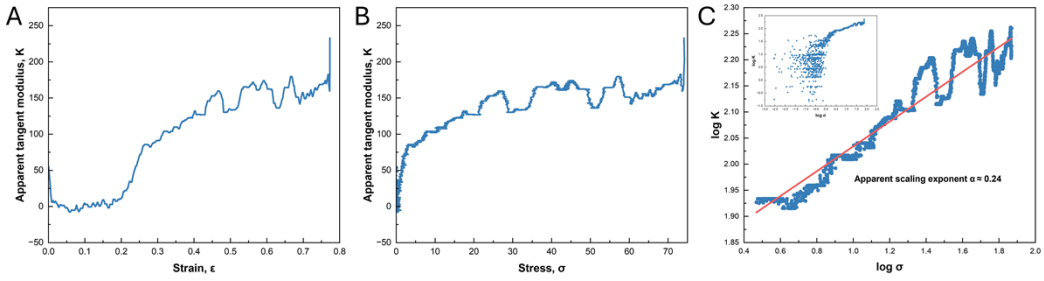

Fig. S3 Apparent tangent modulus analysis of the silk nanofibril network during uniaxial tensile simulation. (A) K plotted as a function of strain. (B) K plotted as a function of stress. (C) Log-log representation of K ersus σ.

References

1 S. Yang, C. Zhao, Y. Yang, J. Ren and S. Ling, ACS Nano, 2023, **17**, 7662–7673.

2 J. Adamcik, J.-M. Jung, J. Flakowski, P. De Los Rios, G. Dietler and R. Mezzenga, Nature Nanotechnology, 2010, **5**, 423–428.

3 J. Adamcik and R. Mezzenga, Macromolecules, 2012, **45**, 1137–1150.

4 C.-T. Lee and M. Merkel, Physical Review E, 2024, **110**, 064147.

5 S. Arzash, A. Gannavarapu and F. C. MacKintosh, Physical Review E, 2023, **108**, 054403.

6 S. Chen, T. Markovich and F. C. MacKintosh, Physical Review Letters, 2024, **133**, 028201.